A New Microstrip Radiator for Medical Applications

I. J. BAHL, MEMBER, IEEE, STANISLAW S. STUCHLY, SENIOR MEMBER, IEEE, AND MARIA A. STUCHLY, SENIOR MEMBER, IEEE

Abstract—**Ring-type microstrip antennas appear to offer important advantages in medical therapy when used for local tissue heating. In designing these radiators, the properties of a microstrip covered with layers of lossy dielectrics representing various tissue layers have to be taken into account. This paper provides basic information on design of ring-type radiators for tissue heating and the experimental results for a unit designed to operate in the TM modes at 2.45 GHz. The radiator is well matched when spaced 1.3–3 mm from muscle tissue or muscle tissue covered by a thin layer of fat tissue. A limited volume of muscle tissue is heated at a greater rate than the fat layer as shown by a thermographic technique.**

I. Introduction

An increased interest in applications of electromagnetic techniques in medical diagnosis and therapy has recently been observed [1], [2]. In therapy, there are indications that local and/or whole body hyperthermia provides successful modality in treatment of some malignant tumors. Microwave energy is one of the effective ways of inducing hyperthermia, but difficulties are experienced in heating deep lying tissues and heating a relatively large volume of tissue. In general, the desired characteristics of a microwave radiator include an effective deposition of the energy in a defined tissue volume (e.g., in the muscle without overheating the skin and fat), good impedance matching, minimum leakage of microwave energy outside of the treated area and lightweight, rugged and easy to handle design.

Microstrip radiators offer the advantage of being small, lightweight and capable of conforming to the shape of the body, when properly designed, with remaining characteristics comparable to those of other microwave radiators used in therapeutic heating. A conformal applicator employing a radiator consisting of a few printed dipoles was previously used for inducing hyperthermia at 2.45 GHz [2]. A coplanar stripline coupler was used in monitoring water content in lungs [3].

A ring-type microwave radiator appears to offer a potential as a local hyperthermia applicator.

Manuscript received May 14, 1980; revised July 18, 1980. This work was supported by the Natural Sciences and Engineering Research Council of Canada.

I. J. Bahl and S. S. Stuchly are with the Department of Electrical Engineering, University of Ottawa, Ottawa, Ontario, Canada K1N 6N5.

M. A. Stuchly is with the Radiation Protection Bureau, Environment Health Center, Health & Welfare Canada, Ottawa, Ontario, Canada K1A 0L2.

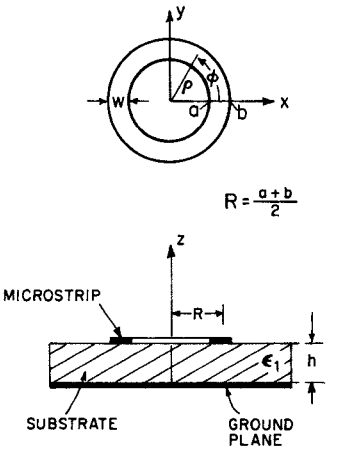

Fig. 1. The geometry of a microstrip ring-type radiator.

In this paper the theory of the operation of a ring-type microstrip radiator when in contact with biological tissue, and design formulas are given. Experimental results including the impedance matching, leakage, and heating patterns obtained by infrared thermography are provided for a radiator designed to operate at 2.45 GHz.

II. Theory and Design Principles

The geometry of a ring microstrip radiator is shown in Fig. 1. The fields inside the region between a ring conductor and a ground plane at resonance for TM modes are as follows [4], [5]:

$$E_z = E_0\left[J_n(k\rho)Y_n'(ka) - J_n'(ka)Y_n(k\rho)\right]\cos n\phi \quad (1)$$

$$H_\rho = \frac{j\omega\epsilon}{k^2\rho}\frac{\partial E_z}{\partial \phi} \quad (2)$$

$$H_\phi = -\frac{j\omega\epsilon}{k^2}\frac{\partial E_z}{\partial \rho} \quad (3)$$

where E_0 is the electric field between the outer edge of the ring and the ground plane at $\phi=0$, n is an integer, $k=2\pi\sqrt{\epsilon_e}/\lambda_0$ (ϵ_e is the effective dielectric constant of the structure and λ_0 is the free space wavelength), and ϵ is the permittivity of the dielectric substrate. J_n and Y_n are Bessel functions of the first and second kind, respectively. The prime sign denotes derivative of Bessel functions. The surface currents on the circular ring can then be found with $K_\phi = -H_\rho$ and $K_\rho = H_\phi$. The radial component of

0018-9480/80/1200-1464$00.75 ©1980 IEEE

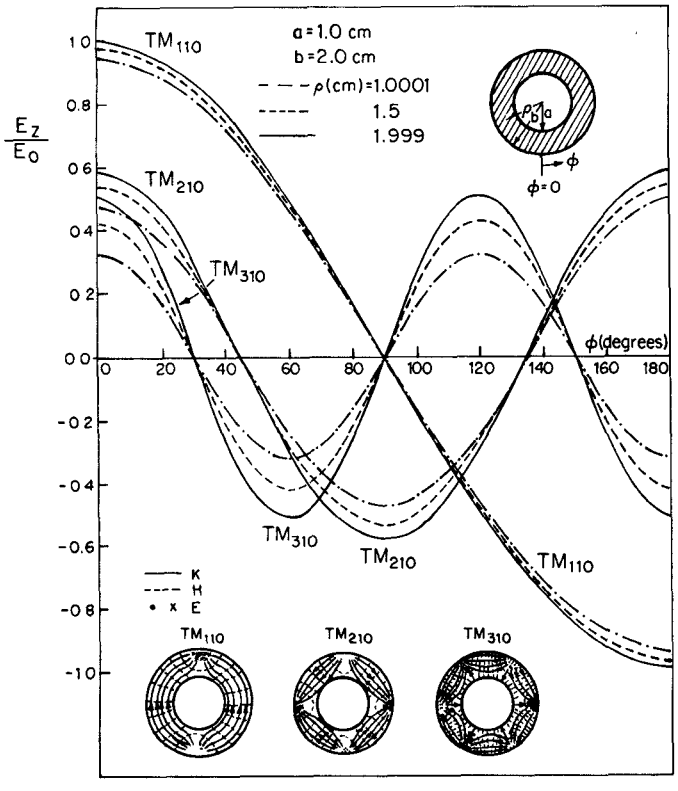

Fig. 2. The field patterns and the normalized electric field intensity for the TM modes in the ring-type radiator.

the current must vanish at the edge of the ring, i.e.,

$$K_\rho(\rho=b)=H_\phi(\rho=b)=0. \tag{4}$$

From (1), (3), and (4)

$$J_n'(kb)Y_n'(ka)-J_n'(ka)Y_n'(kb)=0. \tag{5}$$

Equation (5) allows one to calculate k of consecutive modes for given dimensions of the ring resonator.

The variations of the normalized electric field E_z inside the ring as a function of the azimuth angle are shown in Fig. 2. The magnetic field distribution and the surface currents are also illustrated [5]. It may be noted that the field strength at the outer edge of the ring is higher than at the inner edge. The difference in the field strengths increases with the mode number.

For TM_{n10} modes and $n \leqslant 5$ and $(b-a)/(b+a) \leqslant 0.35$ (Fig. 1), the approximate value of k can be found as equal to

$$k=\frac{2n}{a+b}. \tag{6}$$

The resonant frequency can be calculated as

$$f_0=\frac{ck}{2\pi\sqrt{\epsilon_e}} \tag{7}$$

where c is the velocity of light and ϵ_e is the effective dielectric constant.

A microstrip ring resonator is formed from a microstrip transmission line bent in a circular shape. If the radius of curvature is large compared with the width of the strip,

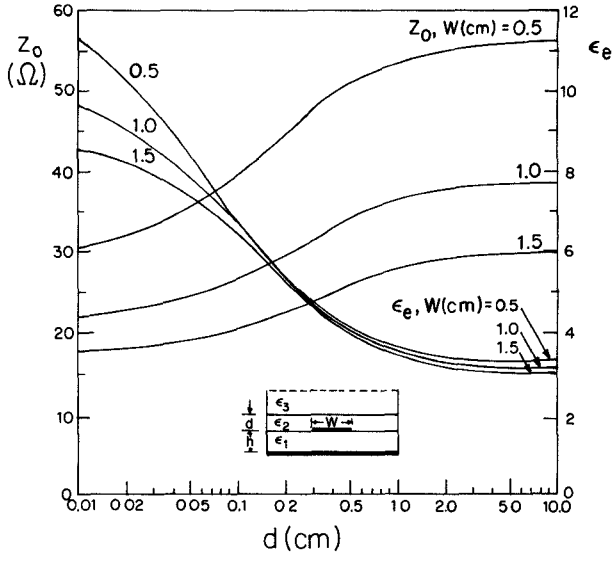

Fig. 3. The effective dielectric constant and characteristic impedance of a microstrip covered with a dielectric layer of thickness d and an infinite dielectric above it; substrate thickness, $h=0.318$ cm, substrate dielectric constant, $\epsilon_{r1}=2.32$, stripwidth $W=0.5$ cm, 1.0 cm, and 1.5 cm, $\epsilon_{r2}=6.0$, $\epsilon_{r3}=50$.

the effective dielectric constant of the ring may be calculated as that of an equivalent microstrip line with the strip width equal to $W=b-a$.

The effective dielectric constant of a microstrip covered with two layers of lossy dielectric material, with the first layer of a finite thickness, and the second (top) layer extending to infinity has previously been derived using the variational method [6]. The variational expression for the line capacitance C has been derived [6] [7] as

$$\frac{1}{C}=\frac{1}{\pi\epsilon_0 Q^2}\int_0^\infty \frac{\tilde{f}^2(\beta)d(\beta h)}{\left[\dfrac{\epsilon_{r2}\tanh\beta d+\epsilon_{r3}}{\epsilon_{r2}+\epsilon_{r3}\tanh\beta d}+\epsilon_{r1}\cosh\beta h\right](\beta h)} \tag{8}$$

where $\tilde{f}(\beta)$ is the Fourier transform of the charge distribution, Q is the total charge on the ring conductor, and ϵ_0 is the free space permittivity. All other symbols are shown in Fig. 3, while

$$\epsilon_{ri}=\epsilon_i/\epsilon_0 \qquad (i=1,2,3) \tag{9}$$

$$\frac{\tilde{f}(\beta)}{Q}=1.6\left\{\frac{\sin(\beta W/2)}{\beta W/2}\right\}+2.4/(\beta W/2)^2\left\{\cos(\beta W/2)-\frac{2\sin(\beta W/2)}{(\beta W/2)}+\frac{\sin^2(\beta W/4)}{(\beta W/4)^2}\right\}. \tag{10}$$

The characteristic impedance Z_0 and effective dielectric constant ϵ_e are calculated from (8) and (10) using the following relations:

$$\epsilon_e=C/C_a \tag{11}$$

$$Z_0=\left(c\sqrt{CC_a}\right)^{-1} \tag{12}$$

where c is the velocity of light and C_a is the line capacitance when all dielectric layers are replaced by air. The above expressions are valid for lossy layered medium when

$$\frac{\omega\epsilon_0\epsilon_e}{\sigma_e} \gg 1 \tag{13}$$

where σ_e is the effective conductivity of the structure which may be expressed as

$$\sigma_e = q_1\sigma_1 + q_2\sigma_2 + (1-q_1-q_2)\sigma_3. \tag{14}$$

Here q_1 and q_2 are the dielectric filling fractions of the substrate and fat, respectively, and σ_1, σ_2, and σ_3 are the conductivities of the substrate, fat, and muscle, respectively.

Below 1 GHz, the factor $\omega\epsilon_0\epsilon_e/\sigma_e$ (left hand side of (13)) decreases with frequency. For example for 500 MHz, $\omega\epsilon_0\epsilon_e/\sigma_e \simeq 3$ and the expressions (8) to (12) are no longer valid. However, for thick layers of fat ($\geqslant 5$ h) the semi-infinite muscle hardly affects the characteristics of the microstrip line covered with the multilayer structure and the theory can be applied to this composite structure.

Fig. 3 shows the relative effective dielectric constant and the characteristic impedance of a microstrip of given dimensions covered with a finite thickness layer of the dielectric material having the permittivity equal to that of the fat tissue ($\epsilon_{r2}=6$), and an infinite thickness layer of the muscle tissue equivalent material ($\epsilon_{r3}=50$). In practice, the muscle tissue dielectric does not need to be of an infinite thickness, but the thickness has to be sufficient that the wave is sufficiently attenuated. It may be noted from this figure that the effective dielectric constant does not change appreciably with the microstrip width for 0.5 cm $\leqslant W \leqslant$ 1.5 cm and for the fat thickness $d > 0.1$ cm. As the absolute values of the permittivities of fat and muscle are nearly constant in the frequency range from 0.5 to 3 GHz, the results presented in Fig. 3 are valid in this frequency range.

Fig. 4 shows the resonant frequencies of the first three modes as a function of fat tissue thickness. The dielectric constants of fat and muscle tissues are assumed here to be constant for frequencies 1–5 GHz. This condition, in practice, is met within 20 percent, however, this is satisfactory since the ring resonator covered by a dielectric having a relatively large loss factor has a relatively small Q-factor.

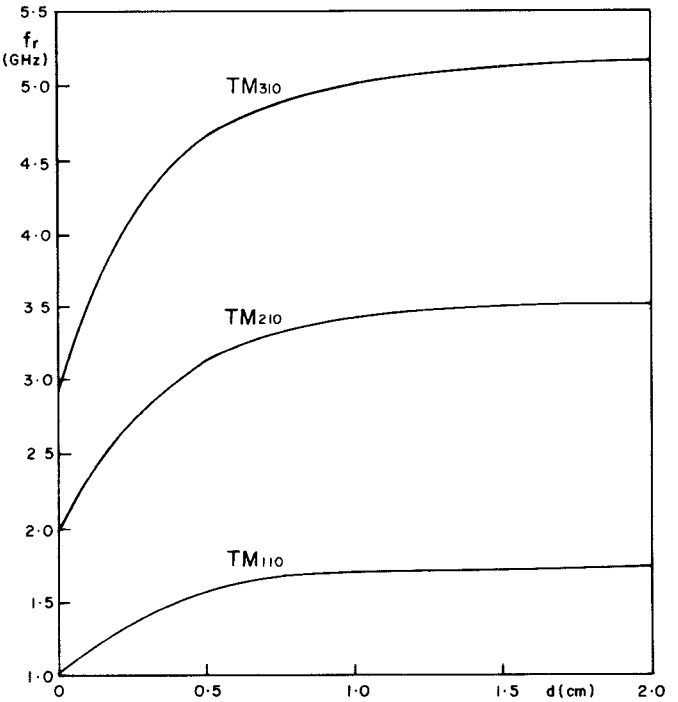

Fig. 4. Resonant frequencies of a ring resonator covered with two layers of dielectric; the first layer has a thickness d and the dielectric constant 6.0, the second layer thickness is infinite and the dielectric constant is 50; the resonator parameters are $a=1$ cm, $b=2$ cm, $h=0.318$ cm, $\epsilon_{r1}=2.32$.

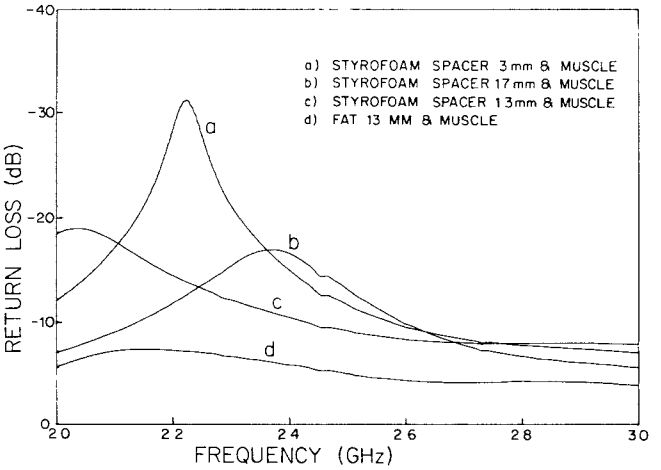

Fig. 5. Return loss for the microstrip radiator as a function of frequency.

III. Experimental Results

A test radiator having $a=1$ cm and $b=2$ cm, on a substrate with $\epsilon_{r1}=2.32$ was designed to operate at 2.45 GHz. The radiator was fed from a coaxial N-type connector through a probe protruding the substrate and in contact with the ring. To provide for cooling of the skin a thin layer of styrofoam (1.3–3 mm) was used to separate the radiator from the tissue. This in effect lowered slightly the effective dielectric constant. The radiator supports the TM_{110} and the TM_{210} modes for muscle tissue covered with a thin layer of fat ($d<0.2$ cm), and only the TM_{110} for thicker layers of fat. This results from the changes in the effective dielectric constant as a function of the fat thickness.

The return loss for the radiator facing muscle, and fat and muscle tissues is shown in Fig. 5 as a function of frequency between 2 and 3 GHz. It may be noted that the structure is well matched especially to muscle tissue in a broad range of frequencies. This latter fact supports the previously drawn conclusion regarding a very low Q-factor of the ring resonator forming the radiator. However, from a practical point of view this is a significant advantage as

it allows for an efficient operation (impedance matching) of the radiator when used for different biological tissues (various fat thickness, nonuniform tissue).

Leakage measured 5 cm from the radiator using an isotropic electric field probe (Narda, model 8631) was below 1 mW/cm^2 per 10 W of net power delivered to the tissue for any styrofoam spacer of a thickness 0–3 mm and fat layer thickness from 0 to 1.25 cm.

Heating patterns were investigated by a thermographic method [8]. A muscle tissue phantom (a jelly-like material consisting of 8.45 percent TX-150, 0.91 percent NaCl, 15.2 percent polyethylene powder and 75.44 percent H_2O [8]) was contained in a styrofoam container having one side open. The muscle phantom formed a right cylinder 10 cm in diameter and 10 cm in height. The open side of the muscle phantom was covered by a plate made of a solid material simulating fat tissue (85.2 percent Laminac 4110, 14.5 percent Aluminium powder, 0.24 percent Acetylene black, 3.75 g/kg MEK Peroxide [8]). The whole phantom (fat, muscle, and container) was divisible along a diameter plane, a thin plastic sheet separated the muscle phantom halves. In all tests the phantom fat or muscle surface was placed in contact with the test radiator and microwave power of 100 W at 2.45 GHz was turned on for 5 s. Immediately after the microwave irradiation a surface of interest was scanned by a thermographic infrared camera. A short exposure time and short delay in recording the surface temperature are essential to limit thermal diffusion. To obtain heating of patterns of the muscle under the fat layer, the fat was removed before the thermographic image was obtained. To obtain "in depth" heating patterns the two halves of the phantom were separated and one of the adjoining surfaces was thermographically scanned. An AGA model 750 camera was employed to obtain temperature images.

Heating patterns obtained at the surface of the muscle phantom and at the surface perpendicular to the ring radiator (the plane of the phantom division), for the radiator separated 1.7 mm from the tissue are shown in Fig. 6(a) and (b), respectively. The same data for the phantom consisting of 1.25 cm of fat simulator and muscle is shown in Fig. 7. Basically the same patterns were obtained for other distances separating the radiator from the tissue (styrofoam layer thicknesses 1.3 and 3 mm). On all thermographs the temperature variation within 5°C in 1°C gradation is shown on a grey scale as black (ΔT= 5°C), white (4°C), light grey (3°C), medium grey (2°C), dark grey (1°C), and black (0°C). Additionally, a bright line indicating the contour having a preselected temperature (isotherm) may be imposed on the thermal image.

The results in Figs. 6 and 7 indicate that a better symmetry of the heating is obtained for the muscle phantom. This may be attributed to the presence of two modes when the radiator is facing muscle and therefore more uniform distribution of the electric field around the ring circumference (Fig. 2). For the fat muscle phantom (Fig. 7(b)), the muscle was heated at a greater rate than the fat.

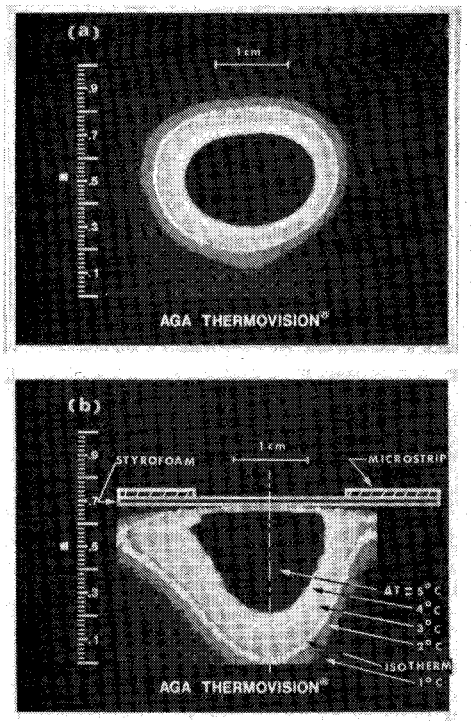

Fig. 6. Heating patterns of the microstrip ring-type radiator at 2.45 GHz. (a) On the surface. (b) In-depth of the simulated muscle tissue. The radiator is separated from the tissue by a 1.7-mm styrofoam layer.

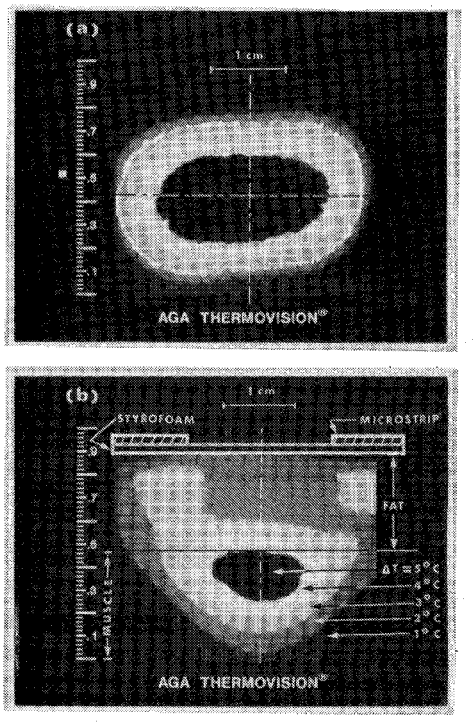

Fig. 7. Heating pattern of the microstrip ring-type radiator at 2.45 GHz. (a) At the muscle–fat interface. (b) In-depth of the simulated tissue consisting of 1.25 cm of fat phantom material and in contact with muscle phantom material. The radiator is separated from the tissue by a 1.7-mm styrofoam layer.

This is of an advantage in practical applications. The heated volume is relatively small, but in this design this is

a desired effect. By selecting a greater radius of the ring, a larger volume would be heated.

IV. Conclusions

The design formulae and experimental results of a 2.45-GHz ring-type microstrip radiator for potential hyperthermia applications are given. Microstrip radiators offer the advantage of being small, lightweight and capable of conforming to the shape of the body. Cooling of the skin is easily accomplished by the air flow through a gap between the skin and the radiator. The preliminary results obtained for a radiator operating at 2.45 GHz are encouraging. A defined volume of muscle can be heated without overheating skin and fat. The energy can be effectively coupled to the tissue, with a relatively small leakage (1 mW/cm^2 per 10 W of net power delivered to the tissue). The heated volume can be controlled by the radiator dimensions. The radiator was designed and tested at 2.45 GHz, because of availability of the test instrumentation, however dimensionally scaled radiators at other frequencies can be designed using the principles described. If at the same time a small cross section of the heated volume is required, a radiator having a substrate of higher dielectric constant can be used.

References

[1] M. F. Iskander and C. H. Durney, "Electromagnetic techniques for medical diagnostics: A Review," *Proc. IEEE*, vol. 68, pp. 126–132, Jan. 1980.
[2] F. Sterzer *et al*, "Microwave apparatus for the treatment of cancer," *Microwave J.*, vol. 23, pp. 39–44, Jan. 1980.
[3] M. F. Iskander and C. H. Durney, "An electromagnetic energy coupler for medical applications," *Proc. IEEE*, vol. 67, pp. 1463–1465, Oct. 1979.
[4] I. Wolff and N. Knoppik, "Microstrip ring resonator and dispersion measurements on microstrip lines," *Electron Lett.*, vol. 7, pp. 779–781, Dec. 1971.
[5] Y. S. Wu and F. J. Rosenbaum, "Mode chart for microstrip ring resonators," *IEEE Trans. Microwave Theory Tech.*, vol. MTT-21, pp. 487–489, July 1973.
[6] I. J. Bahl and S. S. Stuchly, "Analysis of a microstrip covered with a lossy dielectric," *IEEE Trans. Microwave Theory Tech.*, vol. MTT-28, pp. 104–109, Feb. 1980.
[7] E. Yamashita and R. Mittra, "Variational method for the analysis of microstrip lines," *IEEE Trans. Microwave Theory Tech.*, vol. MTT-16, pp. 251–256, Apr. 1968.
[8] A. W. Guy, "Analyses of electromagnetic fields induced in biological tissues by thermographic studies on equivalent phantom models," *IEEE Trans. Microwave Theory Tech.*, vol. MTT-19, pp. 205–215, Feb. 1971.

The Traveling-Wave Divider/Combiner

ALAIN G. BERT AND DIDIER KAMINSKY

***Abstract*—A new kind of distributed power divider/combiner circuit for use in octave (or more) bandwidth microstrip power transistor amplifiers is presented.**

The design, characteristics, and advantages are discussed. Experimental results on a four-way divider and divider/combiner are presented and compared with theory.

First experimental results on a six-way traveling-wave divider (TWD) are also presented.

Introduction

SEVERAL WATTS per chip are now obtainable at *X*-band with power FET's, due to recent improvements in their technology, yet bandwidths remain relatively narrow (20 percent typical). Wider bandwidths may be achieved by the use of internal matching techniques [1]. Nevertheless, the greater the power, the smaller is the input impedance and bandwidth. Therefore, large power values (10 W or more) over octave bandwidths for ECM applications, require wide-band combining circuits.

It must, however, be kept in mind when speaking of combiners, that high-power FET's are already the result of internal power combining. At the chip level, individual FET's are connected in parallel to form a power module. Then a certain number of such modules (generally 2 or 4) are bonded to some capacitances which are part of the input or output matching circuits [2].

Apart from the fact that the input impedance decreases with the number of elements connected in parallel, another reason that there is a limitation in the power of each power FET is related to its longitudinal dimension which becomes comparable to a quarter of a propagation wavelength on the GaAs substrate, particularly when the search for more power is associated with the trend toward high frequencies. A typical value for this longitudinal dimension is 500 $\mu m/W$ of RF power while a quarter of a

Manuscript received May 14, 1980; revised August 2, 1980. This work was supported by the Direction des Recherches, Etudes et Techniques (DRET) under Contract 78/337.

The authors are with Thomson-CSF, Division Composants Micro-ondes, B. P. 10—Domaine de Corbeville, 91401 Orsay, France.

0018-9480/80/1200-1468$00.75 ©1980 IEEE